2

Thermodynamics of Natural and Synthetic Inhibitor Binding to Human Hsp90

Vilma Petrikaitė and Daumantas Matulis
Laboratory of Biothermodynamics and Drug Design, Institute of Biotechnology
Lithuania

1. Introduction

Heat shock protein 90 (Hsp90) is one of conserved heat shock proteins that protect, prevent aggregation, stabilize, activate, or otherwise regulate client proteins, is a component of the cellular chaperone machinery [Taipale et al., 2010, Taldone et al., 2009, Wandinger et al., 2008]. There are a number of recent developments in the understanding of the interesting and complex mechanism of Hsp90 action [Neckers et al., 2009a, Neckers et al., 2009b, Mayer et al., 2009, Walerych et al., 2009]. Hsp90 is over-expressed in cancer cells and Hsp90 inhibitors have shown selectivity for cancer cells. Therefore, small-molecule inhibitors are being developed as anticancer therapeutics [van Montfort and Workman, 2009, Sharp et al., 2007, Sgobba and Rastelli, 2009, Fukuyo et al., 2009].
Two groups of Hsp90 inhibitors have been designed based on naturally occuring inhibitors geldanamycin and radicicol. Geldanamycin has been modified to 17-AAG, while various resorcinol-bearing compounds were designed based on radicicol. Here we describe the thermodynamics of their binding to Hsp90 by isothermal titration calorimetry (ITC) and thermal shift assay (TSA). These assays yield not only the potency, i.e. the Gibbs free energy of binding, but also the enthalpy of binding, the entropy of binding, and the heat capacity of binding. This detailed thermodynamic description and the comparison between homologous compound structures, coupled with structural information of the Hsp90-inhibitor complex, provides insight into the structure-activity relationships (SAR) of the compounds. The SAR helps in the process of rational drug design [Freire, 2009].

2. The structure of Hsp90 and the comparison of human and yeast isoforms

There are several Hsp90 homologs in human, yeast, and bacteria. Human Hsp90 exists in two highly homologous isoforms - α and β. Alpha isoform is prevalent. There are no major known functional differences between the isoforms. Hsp90 homolog in yeast is named Hsc82 and also shares significant homology with human isoforms.
Figure 1 shows the structure of Hsp90 and Hsc82. The protein in solution exists in equilibrium between dimer and monomer. Furthermore, the protein is quite flexible and exists in equilibrium between at least three major conformations [Graf et al., 2009].
The full length protein consists of three major domains – the N-terminal domain (1-216 a.a.), the M-domain (262-524), and the C-terminal domain (525-709). There is also a charged linker (216-262) that did not crystallize and its structure is unknown [Ali et al., 2006]. Inhibitors

such as radicicol and geldanamycin bind to the ATP-binding pocket of Hsp90 and are thus competitive non-covalent inhibitors.

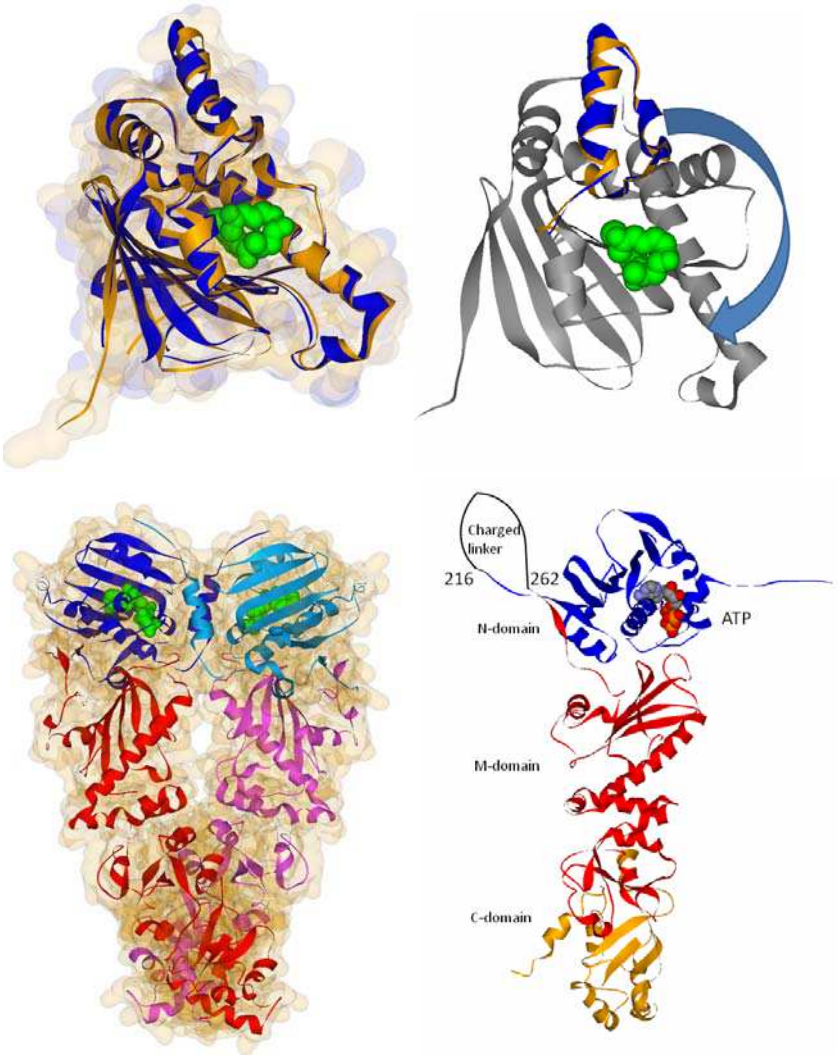

Fig. 1. The structure of Hsp90. Top left. The superimposition of the N-termini of human Hsp90αN (orange) and Hsc82N (blue) with transparent surfaces show that the fold is essentially identical. Radicicol is shown bound to yeast Hsc82N (PDB ID: 1bgq) as spacefilled green model. Top right. Rotation of the 'lid' part of the protein (94-139 a.a., 108-139 a.a. in human Hsp90). Bottom left. The structure of Hsc82 full length dimer (2cg9). One monomer is shown in dark blue-red and another in light blue-pink. Blue shows the position of the N-terminal domains. Bottom right. The structure of Hsc82 full length monomer showing the positions of three domains and the unstructured charged linker

Radicicol interactions with human and yeast Hsp90 isoforms are shown in Figure 2. Crystallographic experimental structure exists only for the yeast isoform. Therefore, radicicol binding to human isoforms was modelled computationally into the active site.

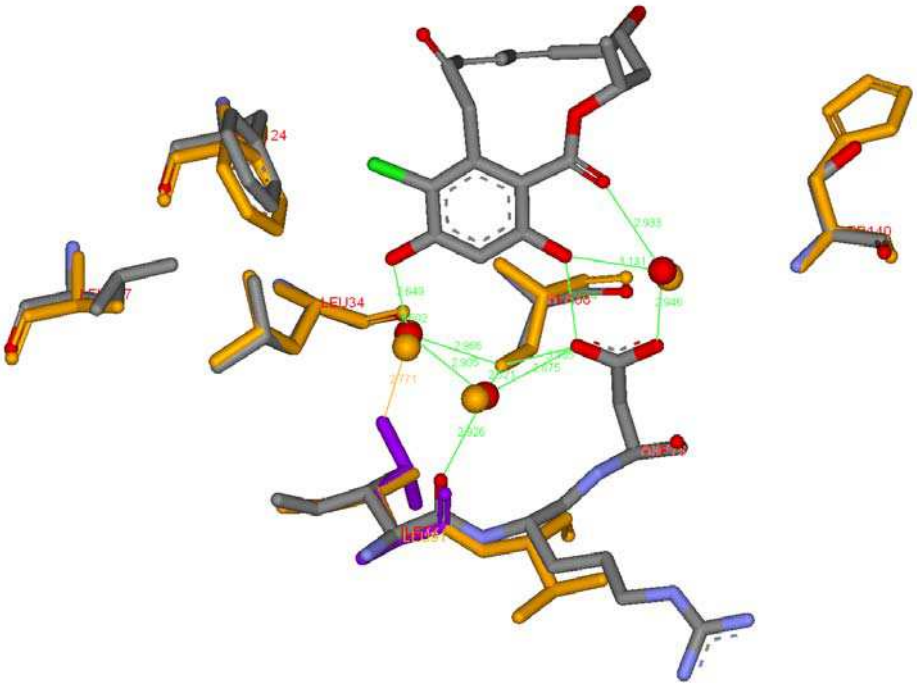

Fig. 2. Interactions of radicicol (grey substance in the middle at the top of the picture) with selected Hsp90 amino acids. Hsp90α amino acids are shown in orange (3eko) superimposed on yeast Hsc82 amino acids (colored by atom, 1bgq), and Hsp90β amino acids are shown in pink. Three important water molecules participating in hydrogen bond formation between the protein and radicicol are shown as spheres

There are very few amino acid differences between yeast and human isoforms that may have an impact on the binding thermodynamics. They are shown in the figure and listed below:

Hsp90α	Ser52	Ile91	Val92	Ala141	His154
Hsp90β	Ala47	Leu86	Val87	Ala136	His149
Hsc82	Ala38	Ile77	Arg78	Leu127	Ser140

All other amino acids in the vicinity of radicicol are identical in all three isoforms. Therefore, the difference in the binding thermodynamics should be due to the above mentioned amino acids. Furthermore, charged amino acids Arg78 and His154 point to the solvent on the

protein surface different from radicicol binding site. Therefore, the difference is most likely due to the remaining three amino acids.

3. Thermodynamics of binding by isothermal titration calorimetry and thermal shift assay

Protein – ligand binding equilibrium is described by the Gibbs free energy of binding ($\Delta_b G$). More negative $\Delta_b G$ indicates a stronger binding reaction. The Gibbs free energy is sufficient to describe the equilibrium. However, several thermodynamic parameters that contribute to the $\Delta_b G$ can be correlated with structural features of the protein – ligand complex easier than the $\Delta_b G$ itself. The most important parameters are the enthalpy ($\Delta_b H$) and entropy ($\Delta_b S$) of binding:

$$\Delta_b G = \Delta_b H - T\Delta_b S \tag{1}$$

Both the enthalpy and entropy are the fist temperature derivatives (T-derivatives) of the Gibbs free energy:

$$\left(\frac{\partial \Delta_b G}{\partial T}\right)_P = -\Delta_b S \tag{2}$$

$$\left(\frac{\partial \ln K_b}{\partial \frac{1}{T}}\right)_P = -\frac{\Delta_b H}{R} \tag{3}$$

The second T-derivative of the $\Delta_b G$ (the $\Delta_b H$ T-derivative) is the heat capacity of binding ($\Delta_b C_P$). Subscript P indicates constant pressure.

$$\Delta_b C_p = \left(\frac{\partial \Delta_b H}{\partial T}\right)_p \tag{4}$$

There are other thermodynamic parameters that are pressure derivatives (P-derivatives) of $\Delta_b G$. The first P-derivative is the volume of binding ($\Delta_b V$). The second P-derivatives are the compressibility and expansion of binding. These parameters may be measured by varying the pressure of the protein – ligand system. However, they are rarely used and are beyond the scope of this chapter. Here we will concentrate on the most used, however, selected thermodynamic parameters, namely, $\Delta_b G$, $\Delta_b H$, $\Delta_b S$, and $\Delta_b C_P$.

The Gibbs free energy of ligand binding may be measured by a large variety of methods, well reviewed for carbonic anhydrase inhibitor binding in [Krishnamurthy et al., 2008]. Here we will concentrate on the application of (ITC) and the (TSA). Both methods have been described previously in detail, especially ITC [Freyer and Lewis, 2008, Landbury, 2004,

Velazquez-Campoy et al., 2004]. However, TSA is rather unconventional and underused despite its great advantages and usefulness [Zubriene et al., 2009, Cimmperman et al., 2008, Matulis et al., 2005].

ITC directly measures the heat evolved or absorbed during the binding reaction. At constant pressure, the heat is equal to the enthalpy ($\Delta_b H$) of binding. This method is the most robust and accurate way of measuring the $\Delta_b H$. However, until the isothermal titration calorimeters became commercially available in early 90s, the $\Delta_b H$ was usually estimated from the $\Delta_b G$ T-dependence using the van't Hoff relationship (3). If all contributing reactions are clearly dissected, such approach should yield the same results as titration calorimetry. However, in practice, there are many unexplained inconsistencies and only ITC provides reliable $\Delta_b H$.

However, the ITC has a number of disadvantages. Most importantly, the binding constant should be in a rather narrow range to satisfy the requirement that coefficient *c* is between about 5 and 500. The *c* is:

$$c = nM_t K_b \tag{5}$$

Where *n* is the binding stoichiometry, M_t is the protein molar concentration, and K_b is the binding constant defined for the reaction of $M + L \rightleftarrows ML$ as:

$$K_b = \frac{[ML]}{[L][M]} \tag{6}$$

$$\Delta G = -RT \ln K_b \tag{7}$$

In practice, ITC is useful for K_bs in the range of 10^5 to 10^9 M^{-1}. Such K_b can be usually measured by varying protein concentration. If ITC experiment is planned well, it can provide $\Delta_b G$, $\Delta_b H$, and $\Delta_b S$ in an hour. Doing the same experiment at several temperatures will yield an indirect measurement of the heat capacity $\Delta_b C_P$.

Another disadvantage of ITC is that it requires rather large amount of protein (usually more than 0.1 mg) and ligand. The protein must be well purified and soluble at micromolar concentrations.

These disadvantages can be quite easily approached using the TSA. This method is based on the observation that specifically binding ligands stabilize (sometimes destabilize) the protein. Protein solution is being heated at a constant rate in the absence or presence of a ligand and the unfolding pattern is measured by various methods such as absorbance, circular dichroism, or, most often, by fluorescence. Various fluorescent components could be followed, such as intrinsic tryptophan fluorescence or an extrinsic solvatochromic probe. Most convenient is 1,8-anilino naphthalene sulfonate (ANS). Figure 3 shows ANS fluorescence dependence on temperature upon Hsp90 unfolding. The rise in fluorescence near 50 °C is due to Hsp90 unfolding and the exposure of hydrophobic patches of the protein interior. ANS binds to such patches and its fluorescence increases.

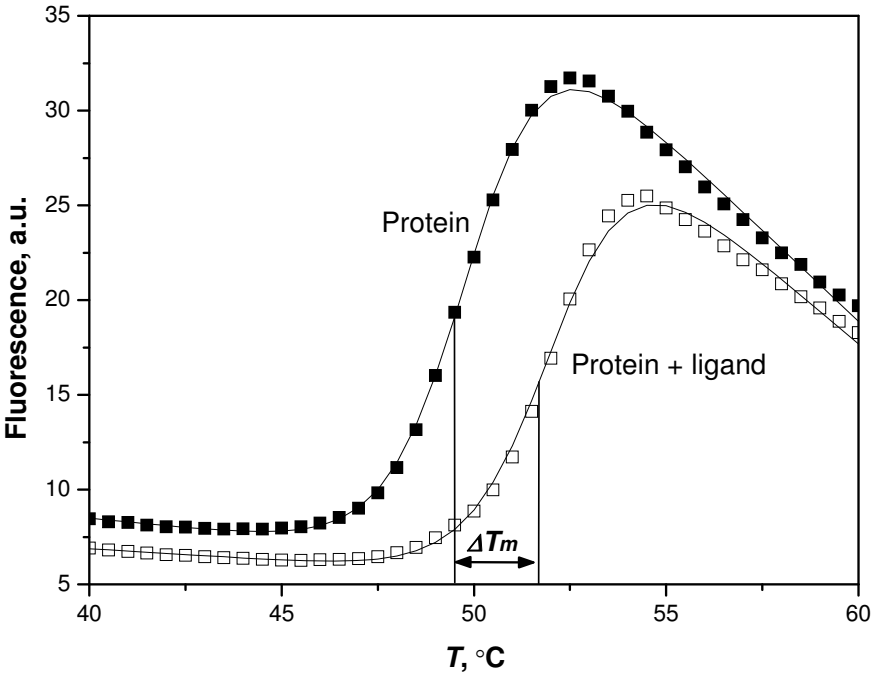

Fig. 3. Thermal shift assay protein melting curves. The midpoint of denaturation (T_m) is shifted to higher temperature upon ligand addition

Note that ANS primarily binds to cationic groups on the protein surface (first to arginine residues) [Matulis and Lovrien, 1998]. However, most such bound ANS does not fluoresce and thus we can observe the unfolding pattern of the protein. Addition of ligand stabilized the protein and shifted the curve and the midpoint of the unfolding transition (T_m) by about 5 degrees.

Protein unfolding fluorescence curves are described by the equation:

$$y = y_{\mathrm{N}} + \frac{y_{\mathrm{U}} - y_{\mathrm{N}}}{1 + e^{\frac{\Delta_u G}{RT}}} = y_{\mathrm{U}} + \frac{y_{\mathrm{N}} - y_{\mathrm{U}}}{1 + e^{-\frac{\Delta_u G}{RT}}} \tag{8}$$

Protein melting temperatures can be determined by fitting the protein melting curves (Figure 3) according to:

$$y(T) = y_{F,T_m} + m_F(T - T_m) + \frac{(y_{\mathrm{U},T_m} - y_{F,T_m}) + (m_U - m_F)(T - T_m)}{1 + e^{\left(\Delta_U H_{T_m} + \Delta_U C_p (T - T_m) - T\left(\Delta_U S_{T_m} + \Delta_U C_p \ln(T/T_m)\right)\right)/RT}} \tag{9}$$

where $y(T)$ is the calculated fluorescence as a function of temperature; y_{F,T_m} is the fluorescence of the probe bound to folded native protein before the transition at T_m; y_{U,T_m} is the fluorescence of the probe bound to the unfolded protein after the unfolding transition at T_m; m_F is the slope of the fluorescence dependence on temperature when the probe is bound to the native protein; m_U is the slope of the fluorescence dependence on temperature when the probe is bound to the unfolded protein; $\Delta_U H_{T_m}$ is the enthalpy of protein unfolding at T_m; $\Delta_U S_{T_m}$ is the entropy of protein unfolding at T_m; $\Delta_U C_p$ is the heat capacity of protein unfolding and is assumed to be temperature-independent over the temperature range studied; R is the universal gas constant; and T is the absolute temperature (Kelvin).

Ligand dosing curves (as in Figures 9 and 10) are described by the equation (10):

$$L_t = (K_{U,T_m} - 1)\left(\frac{P_t}{2K_{U,T_m}} + \frac{1}{K_{b,T_m}}\right) = \left(e^{-\left(\Delta_U H_{T_r} + \Delta_U C_p (T_m - T_r) - T_m\left(\Delta_U S_{T_r} + \Delta_U C_p \ln(T_m/T_r)\right)\right)/RT_m} - 1\right)$$

$$\times\left[\frac{P_t}{2}\frac{1}{e^{-\left(\Delta_U H_{T_r} + \Delta_U C_p (T_m - T_r) - T_m\left(\Delta_U S_{T_r} + \Delta_U C_p \ln(T_m/T_r)\right)\right)/RT_m}} + \frac{1}{e^{-\left(\Delta_b H_{T_0} + \Delta_b C_p (T_m - T_0) - T_m\left(\Delta_b S_{T_0} + \Delta_b C_p \ln(T_m/T_0)\right)\right)/RT_m}}\right]$$

L_t is the total concentration of added ligand, K_{U,T_m} is the protein unfolding equilibrium constant at T_m; P_t is the total protein concentration; K_{b,T_m} is the ligand binding constant at T_m; $\Delta_U H_{T_r}$ is the enthalpy of protein unfolding at T_r; T_r is the protein melting temperature when no ligand is added; $\Delta_U S_{T_r}$ is the entropy of protein unfolding at T_r; $\Delta_U C_p$ is the heat capacity of protein unfolding and is assumed to be temperature-independent over the temperature range studied; $\Delta_b H_{T_0}$ is the enthalpy of ligand binding at T_0; T_0 is the temperature at which the binding process is studied (usually 37 °C); is the entropy of ligand binding at T_0; and $\Delta_b C_p$ is the heat capacity of ligand binding and is assumed to be temperature-independent over the temperature range studied.

The binding constant at the physiological temperature T_0 is determined using:

$$K_{b,T_0} = e^{-\left(\Delta_b H_{T_0} - T_0 \Delta_b S_{T_0}\right)/RT_0} \tag{11}$$

TSA can be performed in the RT-PCR machine and requires only several micrograms of protein. Furthermore, there is no upper limit of the K_b to be determined. The only limit is the temperature of water boiling. Therefore, such extremely tight reactions as radicicol binding to Hsp90 can be studied by TSA. There is also no lower limit for the K_b. Therefore, millimolar and picomolar ligands can be easily measured. However, TSA does not determine $\Delta_b H$, $\Delta_b S$, and $\Delta_b C_p$. Therefore, both TSA and ITC should be used to determine the thermodynamics of Hsp90 – ligand binding.

4. Thermodynamics of Hsp90 ligand binding

Figure 4 shows the structures of Hsp90 ligands used in this study.

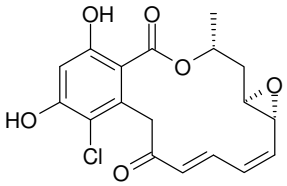

Radicicol

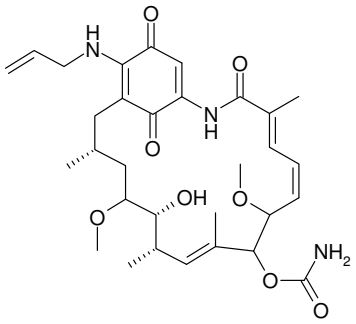

17-AAG

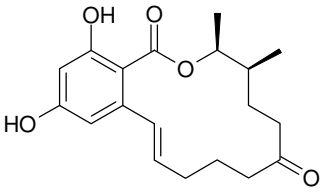

ent-35

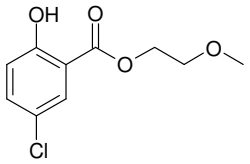

AZ1

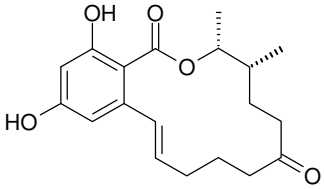

35

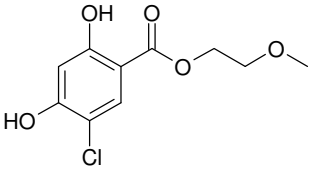

AZ3

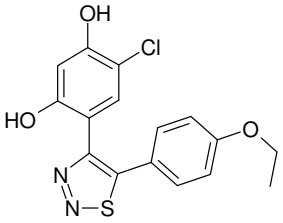

ICPD47

Fig. 4. Chemical structures of compounds discussed in this manuscript

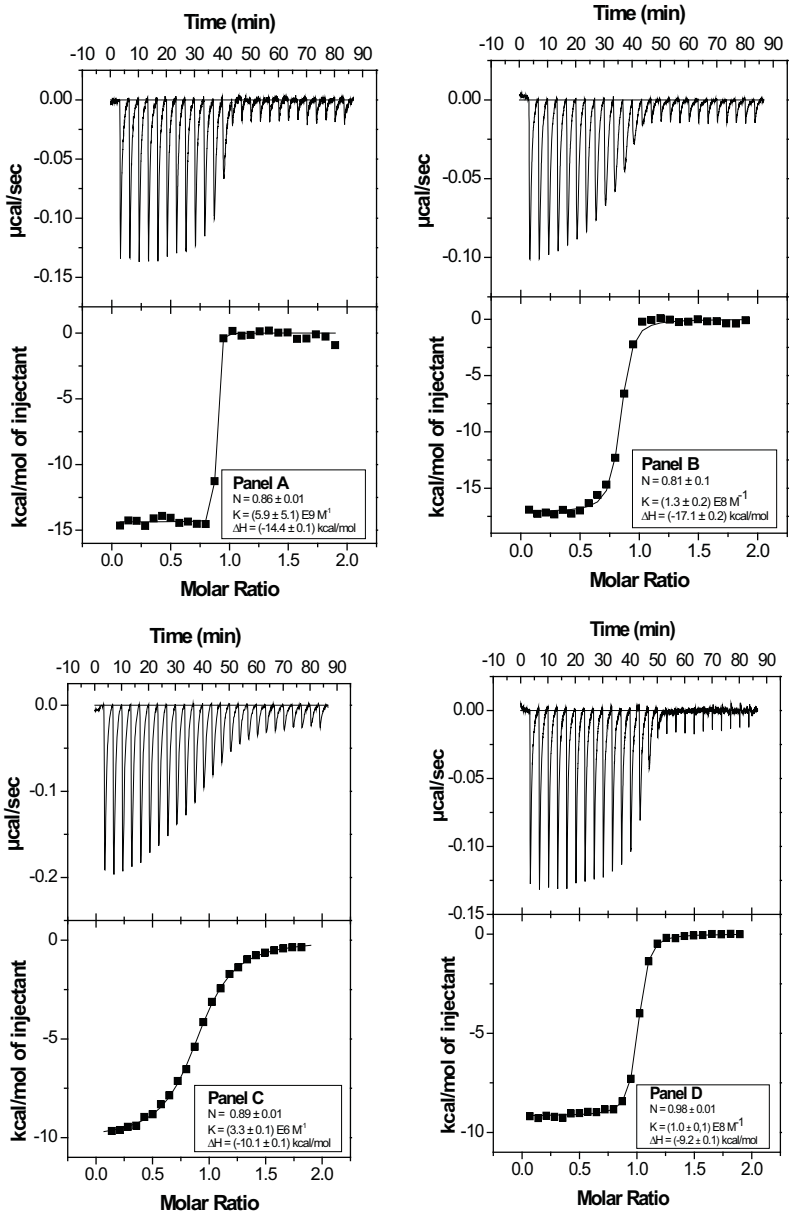

Fig. 5. A. Isothermal titration calorimetry data for radicicol binding to Hsp90αN. Upper graph – raw ITC data, lower graph – integrated ITC data with the curve fit to the standard single binding site model. The cell contained 4 µM protein, while the syringe contained 40 µM radicicol in the same buffer - 50 mM sodium phosphate, pH 7.5, 0.5% DMSO, 100 mM NaCl, at 25 °C. B. Radicicol binding ITC curve at the same conditions as in panel A except pH 8.5. C. 17-AAG binding to Hsp90αN. D. ICPD47 compound binding to Hsp90αN

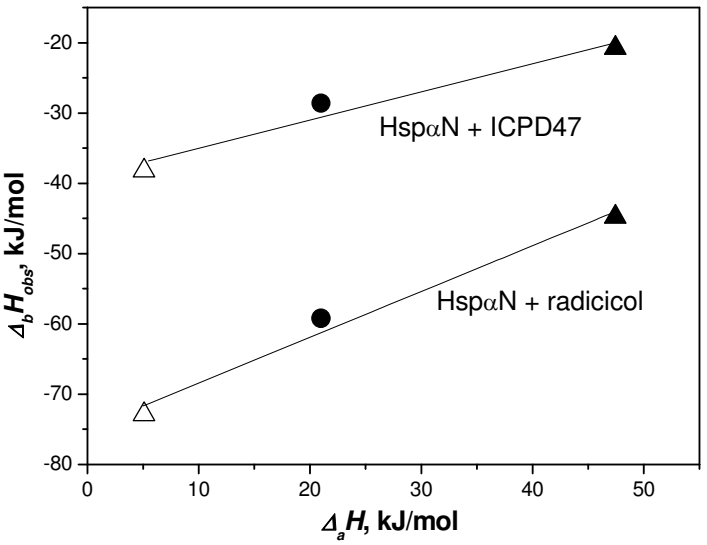

Fig. 6. The observed enthalpies as a function of the buffer deprotonation enthalpy at 25 °C temperature in various buffers: △ – phosphate, ● – Hepes, ▲ - Tris. The data points are the experimentally-observed enthalpies, and the trendlines are linear fits. Their slopes are equal to the binding-linked protonation events. Intersection with y axis is buffer-independent binding enthalpy

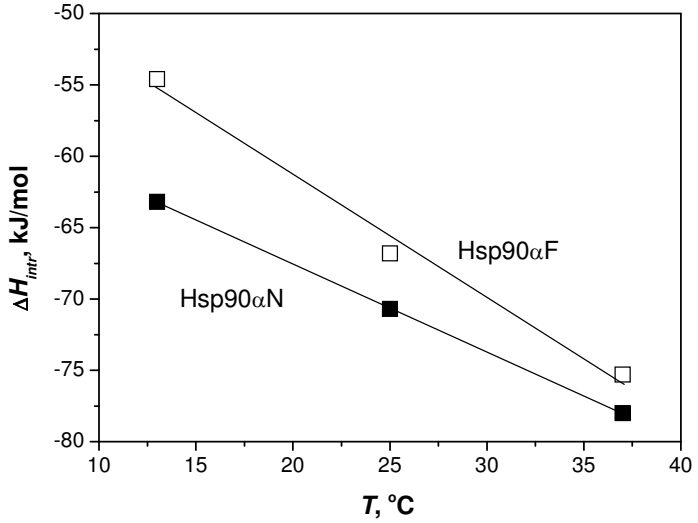

Fig. 7. Intrinsic binding enthalpies obtained after accounting for the linked protonation event as a function of temperature for radicicol binding to Hsp90αN (■) and Hsp90αF (□). The slopes are linear fits to the experimental data and are equal to the intrinsic heat capacities of radicicol binding

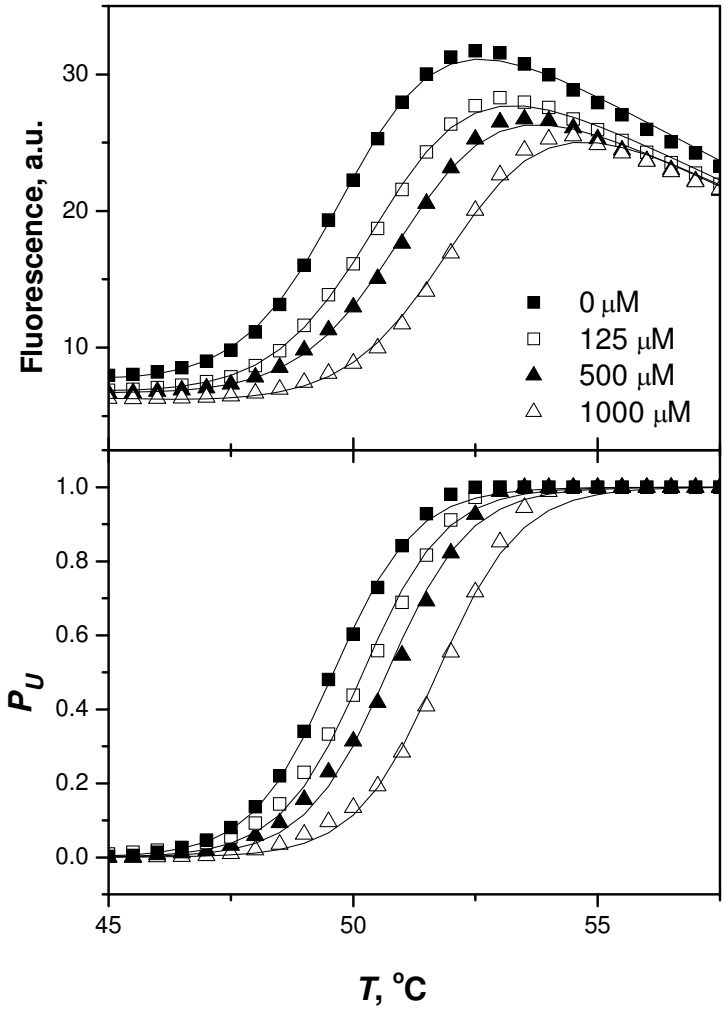

Fig. 8. The binding of AZ3 to Hsp90αN at pH 7.0 as determined by the thermal shift assay. Upper panel shows experimental fluorescence curves. The lower panel shows the same curves recalculated as probabilities to observe the protein in the denatured state

Figure 5 shows several typical ITC binding curves of the Hsp90 – ligand system. The curve in panel A is too steep, meaning that radicicol binding is too tight to be accurately determined by ITC. TSA data will be needed to determine the K_b and $\Delta_b G$ of interaction. However the $\Delta_b H$ is determined to high precision.

The $\Delta_b H$ determined in buffers with different enthalpy of protonation ($\Delta_a H$) yielded different $\Delta_b H$ (Figure 6). Therefore, the binding reaction is linked with protein or ligand protonation or deprotonation upon binding. In other words, ligand binding shifts the pK_a of ionisable groups as previous explained [Baker and Murphy, 1996].

Due the linked protonation, it is important to dissect protonation thermodynamics from binding thermodynamics in order to determine the intrinsic thermodynamics of binding. The enthalpy of, for example, Tris buffer protonation is so large (about -44 kJ/mol) that it would hide any binding enthalpies. Therefore, a series of experiments in various buffers are necessary (Figure 6).

When protonation-linkage effects are accounted for [Zubriene et al., 2010] and the intrinsic enthalpy of binding is determined, such experiments should be repeated at all temperatures of interest. Figure 7 shows intrinsic enthalpies determined at 13, 25, and 37 °C for radicicol-Hsp90α system. The full length protein bound radicicol with slightly less exothermic enthalpy. The difference was equal to ~ 4 kJ/mol (Table 1). This difference is within the standard error of the measurements. The error was greater for the full length protein because the available protein amount and concentration was lower.

ITC was useful to provide the enthalpy of binding. However, as seen in radicicol binding ITC curves in Figure 5, the binding is too tight and would require the displacement assay as described previously [Velazquez-Campoy and Freire, 2006]. Our experience shows that the TSA is much easier and yields more precise results than the displacement ITC assay [Zubriene et al., 2009].

Therefore, the binding of all ligands listed in Figure 4, was measured by the TSA. Figure 8 shows typical raw protein melting curves observed at various added ligand concentration. AZ3 bound with relatively low, millimolar affinity. Therefore, relatively large concentration of ligand had to be added in order to observe the T_m shift.

It should be noted here that the shift continues way beyond saturation of protein with ligand. This is due to the dominant entropy of mixing. If the stabilization occurred due to some kind of bond formation, then we would not observe continued stabilization past the saturation point. This is observed when an inhibitor binds covalently and irreversibly to the protein.

Figures 9 and 10 show the dosing curves for the ligands listed in Figure 4. Radicicol, the most potent binder, shifts the temperature by nearly 15 °C. 17-AAG is the average binder and shifts the temperature by about 10 °C. Some ligands, such as AZ1, barely shift the temperature even at 1 mM concentration.

Protein	K_d, nM	$\Delta_b H_{intr}$, kJ×mol^{-1}	$\Delta_b G_{intr}$, kJ×mol^{-1}	$T\Delta_b S_{intr}$, kJ×mol^{-1}	$\Delta_b S_{intr}$, J×mol^{-1}×K^{-1}	$\Delta_b C_p$, J×mol^{-1}×K^{-1}
Hsp90αN	0.04	-70.7	-59.4	-11.4	-38	-620
Hsp90αF	0.04	-66.8	-59.4	-7.5	-25	-860
Hsp90βN	0.15	-60.6	-56.1	-4.6	-15	-760
Hsc82F	0.25	-46.7	-54.8	8.1	27.1	-620
Uncertainties	±1.6-fold	±4	±2.6	±4.7	±16	±140

Table 1. Intrinsic thermodynamic parameters of radicicol binding to human ant yeast isoforms of Hsp90

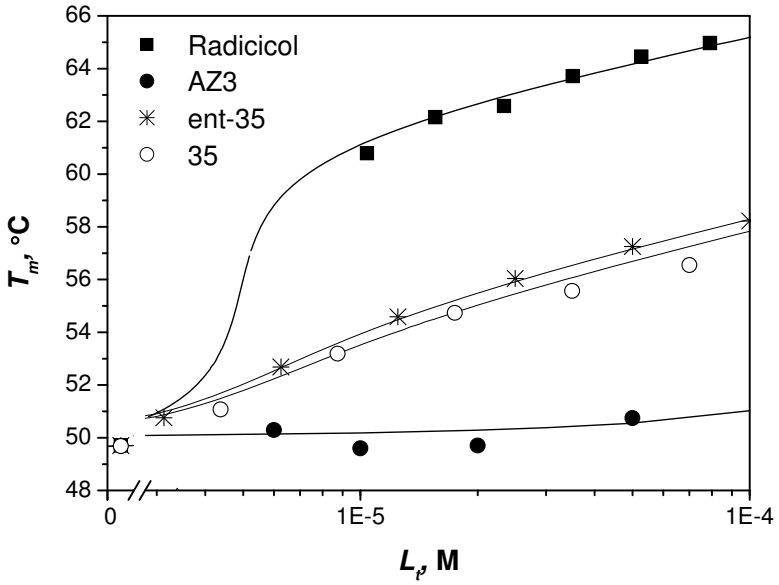

Fig. 9. The dependence of the melting temperature of Hsp90αN on the concentration of various inhibitors (ligand dosing curves) [Ugele et al., 2009]. The observed K_ds (μM) by TSA were: Radicicol – 0.00083, AZ3 – 5000, *ent*-35 – 0.27, and 35 – 0.4

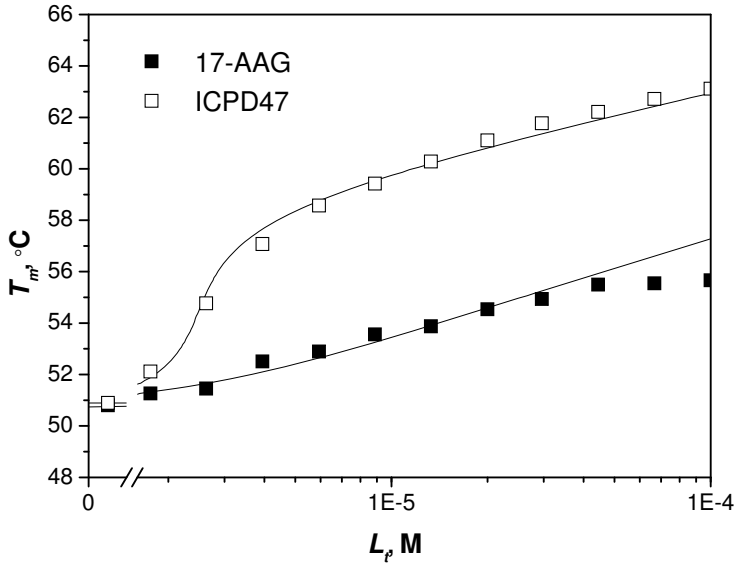

Fig. 10. The dependence of the melting temperature of Hsp90α N on the concentration of inhibitors 17-AAG and ICPD47. The observed K_ds (μM) by TSA were: 17-AAG – 0.3 and ICPD47 – 0.002

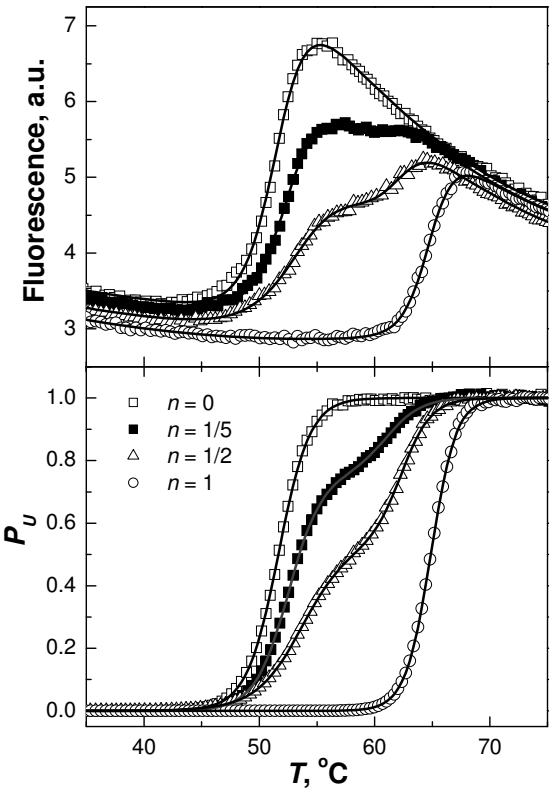

Fig. 11. Denaturation profiles of Hsp90αN in the presence of various radicicol concentrations [Zubriene et al., 2009]

Figure 11 shows an interesting phenomenon observed in TSA when the concentration of ligand is lower than protein. When the concentration of ligand is insufficient to saturate all protein binding sites, the denaturation transition splits into two transitions – the first transition is due to free protein and the second is due to the liganded protein. Relative magnitudes of both transitions are proportional to the concentrations of free and liganded protein concentrations. This phenomenon has been also observed by DSC with weakly-binding ligands at relatively high protein concentrations [Sharke and Ross, 1988].

TSA enabled determination of sub-nanomolar binding potency of naturally occuring radicicol and strongly or weakly-binding synthetic compounds where ITC does not work. However, no dissection of proton linkage was done for ligands where ITC was not feasible. Therefore, only observed K_ds are obtained for such ligands without other thermodynamic information. After dissecting the proton linkage by ITC, it was shown that radicicol binds about 4 times more strongly to recombinant human Hsp90 alpha than to Hsp90 beta isoform. This reduction in affinity is caused primarily by less favorable enthalpic rather than entropic contributions. About 90% of the binding energy comes from the favorable enthalpic contribution and small opposing entropic contribution at physiological temperature (Table 1).

Detailed proton linkage and temperature analysis had to be performed to dissect buffer and protein linked reactions from ligand binding intrinsic reaction. However, even after this

detailed analysis, it is not possible to determine whether conformational change in the protein could contribute significantly to these intrinsic thermodynamic parameters. It is quite likely that some contribution comes from the rotation of the lid as shown in Figure 1. The intrinsic enthalpy of radicicol binding to Hsp90 is one of the largest enthalpies observed for any protein – small ligand binding. Note, that most of the Gibbs free energy of radicicol binding comes from the favourable enthalpic contribution. The entropy contribution is relatively small.

5. Conclusions

Radicicol and other resorcinol-bearing compound binding to Hsp90 is interesting in many respects regarding drug design. First, the binding reaction can be very tight (i.e., it has a very favorable Gibbs free energy). Radicicol stabilizes Hsp90 by 15-20°C. Second, the binding reaction has a very favorable enthalpy of binding, one of the largest for any protein – small ligand system. Third, there are few direct contacts between Hsp90 and radicicol that could account for such a large binding energy. Fourth, water molecules play an essential role in the recognition and binding. And fifth, the negative heat capacity of binding usually reflects a dominant hydrophobic origin of binding. However, hydrogen bonds are apparently essential for radicicol binding to Hsp90.

6. Acknowledgments

The project was supported in part by EEA and Norway Grants 2004-LT0019-IP-1EEE and the Lithuanian Government.

7. References

Ali, M. M., Roe, S. M., Vaughan, C. K., Meyer, P., Panaretou, B., Piper, P. W., Prodromou, C., and Pearl, L. H., 2006. Crystal structure of an Hsp90-nucleotide-p23/sba1 closed chaperone complex. *Nature*, 440(7087):1013–7.

Baker, B. M. and Murphy, K. P., 1996. Evaluation of linked protonation effects in protein binding reactions using isothermal titration calorimetry. *Biophys. J*, 71(4):2049–55.

Cimmperman, P., Baranauskiene, L., Jachimoviciute, S., Jachno, J., Torresan, J., Michailoviene, V., Matuliene, J., Sereikaite, J., Bumelis, V., and Matulis, D., 2008. A quantitative model of thermal stabilization and destabilization of proteins by ligands. *Biophys J*, 95(7):3222–3231.

Freire, E., 2009. A thermodynamic approach to the affinity optimization of drug candidates. *Chem Biol Drug Des*, 74(5):468–72.

Freyer, M. W. and Lewis, E. A., 2008. Isothermal titration calorimetry: experimental design, data analysis, and probing macromolecule/ligand binding and kinetic interactions. *Methods Cell Biol*, 84:79–113.

Fukuyo, Y., Hunt, C. R., and Horikoshi, N., 2009. Geldanamycin and its anti-cancer activities. *Cancer Lett*, 290(1):24-35.

Graf, C., Stankiewicz, M., Kramer, G., and Mayer, M. P., 2009. Spatially and kinetically resolved changes in the conformational dynamics of the hsp90 chaperone machine. *Embo J*, 28(5):602–13.

Krishnamurthy, V. M., Kaufman, G. K., Urbach, A. R., Gitlin, I., Gudiksen, K. L., Weibel, D. B., and Whitesides, G. M., 2008. Carbonic anhydrase as a model for biophysical

and physical-organic studies of proteins and protein-ligand binding. *Chem Rev*, 108(3):946–1051.

Ladbury, J. E., 2004. Application of isothermal titration calorimetry in the biological sciences: things are heating up! *Biotechniques*, 37(6):885–7.

Matulis, D., Kranz, J. K., Salemme, F. R., and Todd, M. J., 2005. Thermodynamic stability of carbonic anhydrase: measurements of binding affinity and stoichiometry using thermofluor. *Biochemistry*, 44(13):5258–66.

Matulis, D. and Lovrien, R., 1998. 1-anilino-8-naphthalene sulfonate anion-protein binding depends primarily on ion pair formation. *Biophys J*, 74(1):422–9.

Mayer, M. P., Prodromou, C., and Frydman, J., 2009. The Hsp90 mosaic: a picture emerges. *Nat Struct Mol Biol*, 16(1):2–6.

Neckers, L., Mollapour, M., and Tsutsumi, S., 2009a. The complex dance of the molecular chaperone Hsp90. *Trends Biochem Sci*, 34(5):223-6.

Neckers, L., Tsutsumi, S., and Mollapour, M., 2009b. Visualizing the twists and turns of a molecular chaperone. *Nat Struct Mol Biol*, 16(3):235–6.

Sgobba, M. and Rastelli, G., 2009. Structure-based and *in silico* design of Hsp90 inhibitors. *ChemMedChem*, 4(9):1399–409.

Sharp, S. Y., Boxall, K., Rowlands, M., Prodromou, C., Roe, S. M., Maloney, A., Powers, M., Clarke, P. A., Box, G., Sanderson, S., *et al*., 2007. In vitro biological characterization of a novel, synthetic diaryl pyrazole resorcinol class of heat shock protein 90 inhibitors. *Cancer Res*, 67(5):2206–16.

Shrake, A. and Ross, P. D., 1988. Biphasic denaturation of human albumin due to ligand redistribution during unfolding. *J Biol Chem*, 263(30):15392–9.

Taipale, M., Jarosz, D.F., Lindquist, S., 2010. HSP90 at the hub of protein homeostasis: emerging mechanistic insights. *Nat Rev Mol Cell Biol*, 11:515-28.

Taldone, T., Sun, W., and Chiosis, G., 2009. Discovery and development of heat shock protein 90 inhibitors. *Bioorg Med Chem*, 17(6):2225–35.

Ugele, M., Sasse, F., Knapp, S., Fedorov, O., Zubriene, A., Matulis, D., and Maier, M. E., 2009. Propionate analogues of zearalenone bind to Hsp90. *Chembiochem*, 10(13):2203-12.

van Montfort, R. L. and Workman, P., 2009. Structure-based design of molecular cancer therapeutics. *Trends Biotechnol*, 27(5):315–28.

Velazquez-Campoy, A. and Freire, E., 2006. Isothermal titration calorimetry to determine association constants for high-affinity ligands. *Nat Protoc*, 1(1):186–91.

Velazquez-Campoy, A., Ohtaka, H., Nezami, A., Muzammil, S., and Freire, E., 2004. Isothermal titration calorimetry. *Curr Protoc Cell Biol*, Ch. 17:Unit 17. 8.

Walerych, D., Olszewski, M. B., Gutkowska, M., Helwak, A., Zylicz, M., and Zylicz, A., 2009. Hsp70 molecular chaperones are required to support p53 tumor suppressor activity under stress conditions. *Oncogene*, 28(48):4284–94.

Wandinger, S. K., Richter, K., and Buchner, J., 2008. The Hsp90 chaperone machinery. *J Biol Chem*, 283(27):18473–7.

Zubrienė, A., Gutkowska, M., Matulienė, J., Chaleckis, R., Michailovienė, V., Voroncova, A., Venclovas, Č., Zylicz, A., Zylicz, M., and Matulis, D. 2010. Thermodynamics of radicicol binding to human Hsp90 alpha and beta isoforms. *Biophys Chem. In press*.

Zubriene, A., Matuliene, J., Baranauskiene, L., Jachno, J., Torresan, J., Michailoviene, V., Cimmperman, P., and Matulis, D., 2009. Measurement of nanomolar dissociation constants by titration calorimetry and thermal shift assay - radicicol binding to Hsp90 and ethoxzolamide binding to CAII. *Int J Mol Sci*, 10(6):2662–2680.

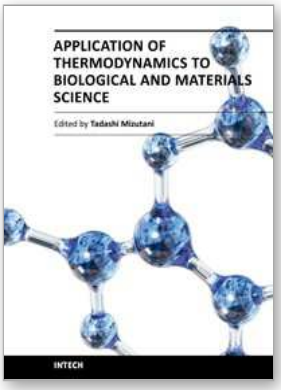

Application of Thermodynamics to Biological and Materials Science

Edited by Prof. Mizutani Tadashi

ISBN 978-953-307-980-6
Hard cover, 628 pages
Publisher InTech
Published online 14, January, 2011
Published in print edition January, 2011

Progress of thermodynamics has been stimulated by the findings of a variety of fields of science and technology. The principles of thermodynamics are so general that the application is widespread to such fields as solid state physics, chemistry, biology, astronomical science, materials science, and chemical engineering. The contents of this book should be of help to many scientists and engineers.

How to reference

In order to correctly reference this scholarly work, feel free to copy and paste the following:

Vilma Petrikaite and Daumantas Matulis (2011). Thermodynamics of Natural and Synthetic Inhibitor Binding to Human Hsp90, Application of Thermodynamics to Biological and Materials Science, Prof. Mizutani Tadashi (Ed.), ISBN: 978-953-307-980-6, InTech, Available from: http://www.intechopen.com/books/application-of-thermodynamics-to-biological-and-materials-science/thermodynamics-of-natural-and-synthetic-inhibitor-binding-to-human-hsp90

INTECH
open science | open minds

InTech Europe
University Campus STeP Ri
Slavka Krautzeka 83/A
51000 Rijeka, Croatia
Phone: +385 (51) 770 447
Fax: +385 (51) 686 166
www.intechopen.com

InTech China
Unit 405, Office Block, Hotel Equatorial Shanghai
No.65, Yan An Road (West), Shanghai, 200040, China
中国上海市延安西路65号上海国际贵都大饭店办公楼405单元
Phone: +86-21-62489820
Fax: +86-21-62489821